

Supplemental Information

HDAC3 is a master regulator of mTEC development

Yael Goldfarb^{1,4}, Noam Kadouri^{1,4}, Ben Levi¹, Asaf Sela¹, Yonatan Herzig¹, Ronald N Cohen², Anthony Hollenberg³ & Jakub Abramson^{1,5}

¹Department of Immunology, Weizmann Institute of Science, Rehovot 76100 Israel

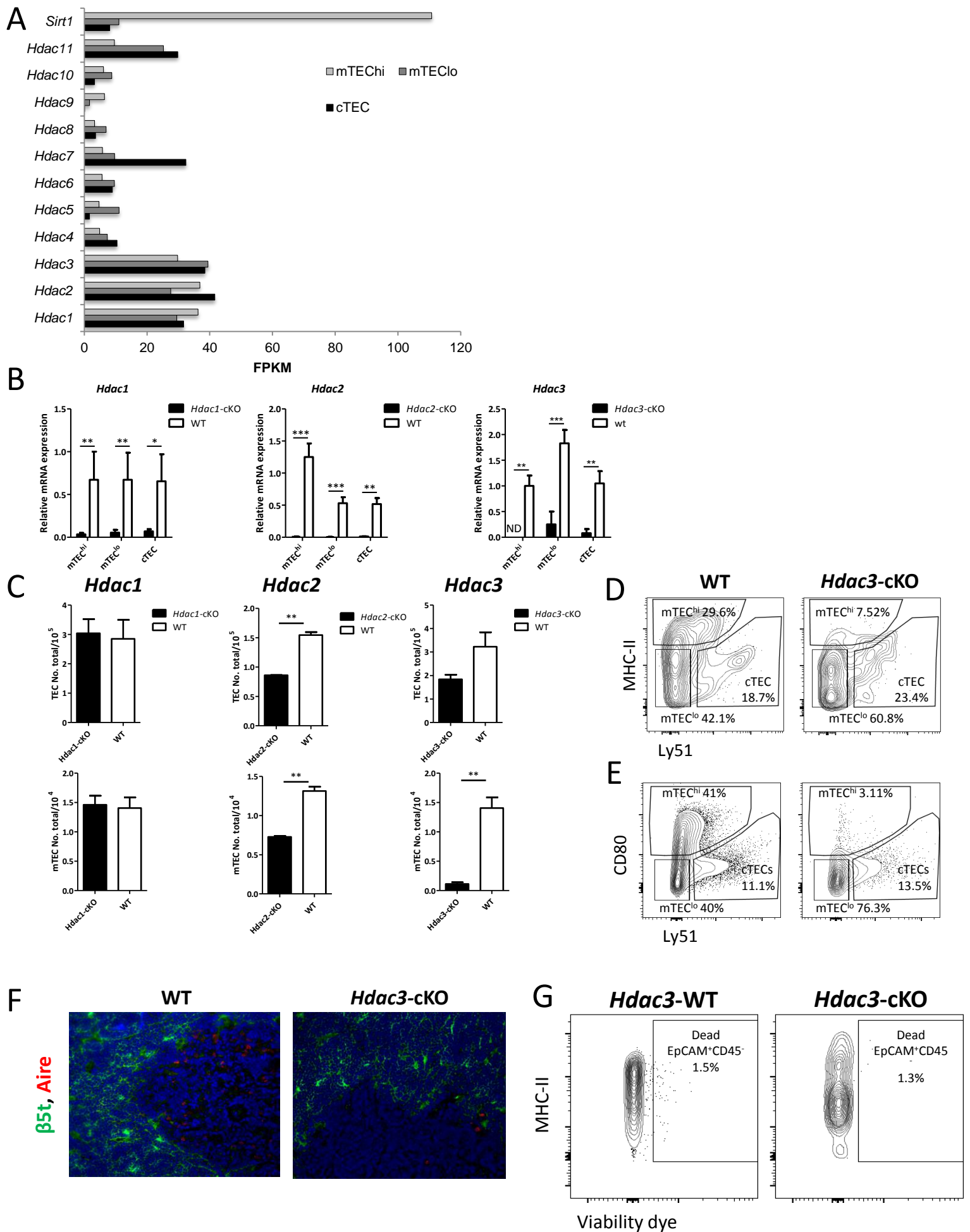
²University of Chicago Medical Centre, Chicago, IL 60637, USA

³Division of Endocrinology, Beth Israel Deaconess Medical Centre, Boston, MA 02215, USA

⁴ Equal contributions

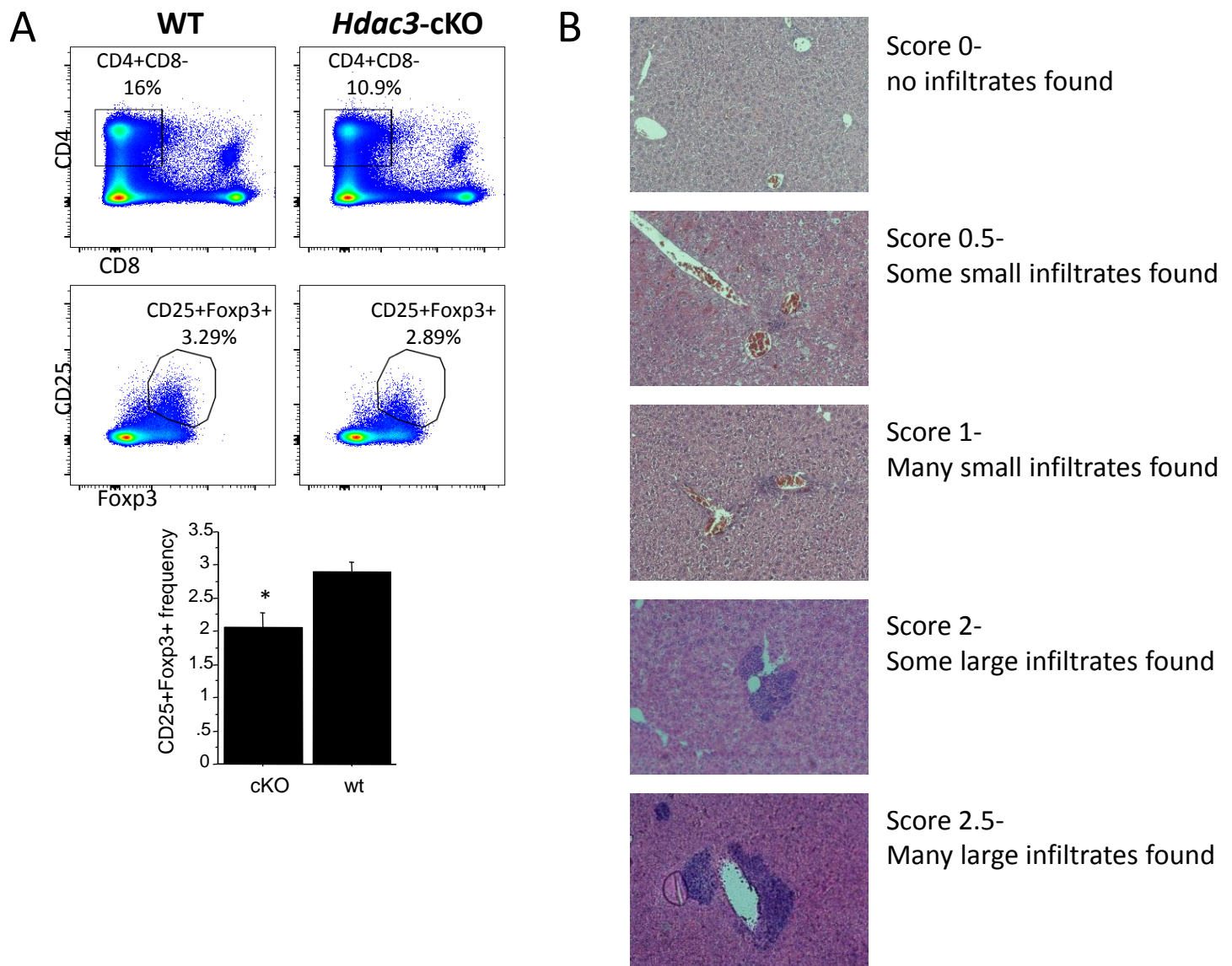
⁵ Correspondence should be addressed to JA (jakub.abramson@weizmann.ac.il)

Figure S1. Related to Figure 1



Suppl. Figure 1, related to Figure 1. (a) Expression of genes encoding histone and protein deacetylases in mTEC^{hi}, mTEC^{lo} and cTECs, assessed by RNA sequencing and presented as fragments per kilobase of transcript per million mapped reads (FPKM). **(b)** qPCR analysis of Foxn1.Cre-mediated recombination efficacy of *Hdac1^{fl/fl}*, *Hdac2^{fl/fl}* and *Hdac3^{fl/fl}* loci. The analysis shows relative mRNA expression + SEM of the corresponding *Hdacs* in sorted mTEC^{hi}, mTEC^{lo} and cTEC populations isolated from either *Foxn1*.Cre-negative (WT; white) or *Foxn1*.Cre-positive (cKO, black) *Hdac1^{fl/fl}*, *Hdac2^{fl/fl}* and *Hdac3^{fl/fl}* mice. Data were normalized to *Hprt* mRNA levels. Asterisks indicate significant differences (**p < 0.001). **(c)** Total cell numbers of the TEC (upper panel) or mTEC (lower panels) compartments of WT *Hdac1^{fl/fl}*, *Hdac2^{fl/fl}* and *Hdac3^{fl/fl}* or their cKO counterparts. **(d)** Representative flow cytometric profile showing frequencies of individual TEC populations from *Hdac3*-cKO and mice and their WT littermates. The displayed cells were first gated on CD45⁻EpCAM⁺ cells (Fig. 1B) and then according to MHC-II or **(e)** CD80 and Ly51 expression to highlight medullary (mTEC) and cortical (cTEC) populations. Individual gates indicate cortical (cTECs) and medullary (mTECs) epithelial cells either high (mTEC^{hi}) or dim (mTEC^{lo}) for MHC-II and CD80 molecule expression. **(f)** Representative staining of frozen thymic sections (20× magnification) from WT and *Hdac3*-cKO mice. β5t staining (green) highlights cortical regions, DAPI staining (blue) highlights cell nuclei and is typically more intense in the cortex, Aire staining (red). **(g)** Representative staining of the thymic stroma (CD45⁻EpCAM⁺ cells) isolated from *Hdac3*-cKO and WT littermates with viability dye and MHC-II.

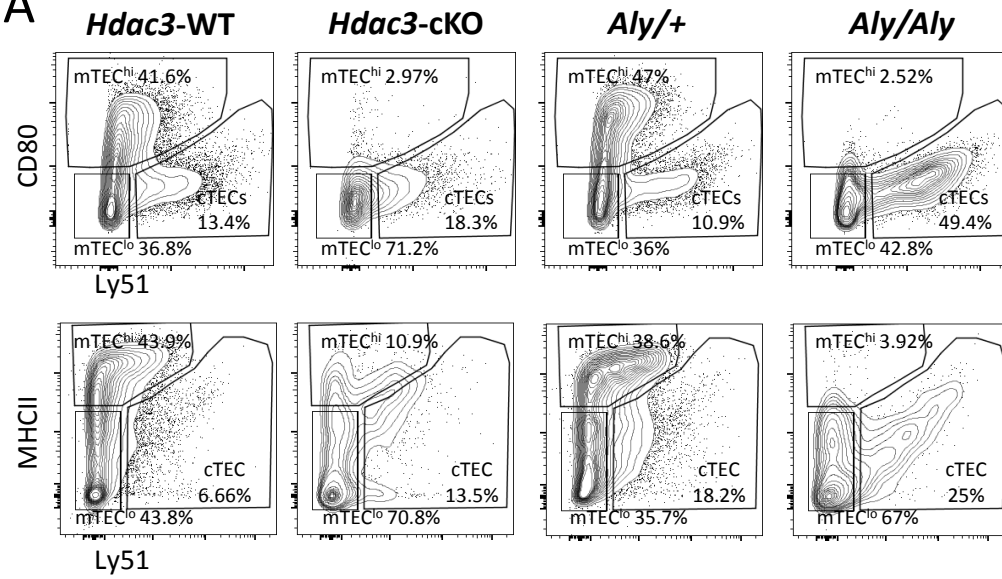
Figure S2. Related to Figure 2



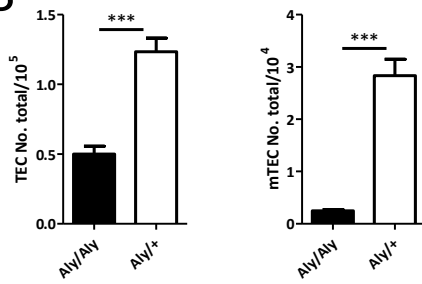
Suppl. Figure 2, related to Figure 2. (a) Representative flow cytometric profile showing frequencies of CD4/CD8 splenocytes (upper panel) and CD4⁺CD25⁺Foxp3⁺ T_{reg} cells (lower panel) obtained from 5-week-old WT and *Hdac3*-cKO spleens, as well as respective graphs showing average frequencies + SEM of CD4⁺CD25⁺Foxp3⁺ T_{reg} cells isolated from WT (white) and *Hdac3*-cKO mice (black); Average values are calculated from three WT and three *Hdac3*-cKO animals, asterisks indicate significant differences (**p* < 0.05). (b) Hematoxylin and eosin (H&E) staining of paraffin embedded sections of livers from aged WT or *Hdac3*-cKO mice representing the scoring system used for assessing immune cell infiltration.

Figure S3. Related to Figure 3

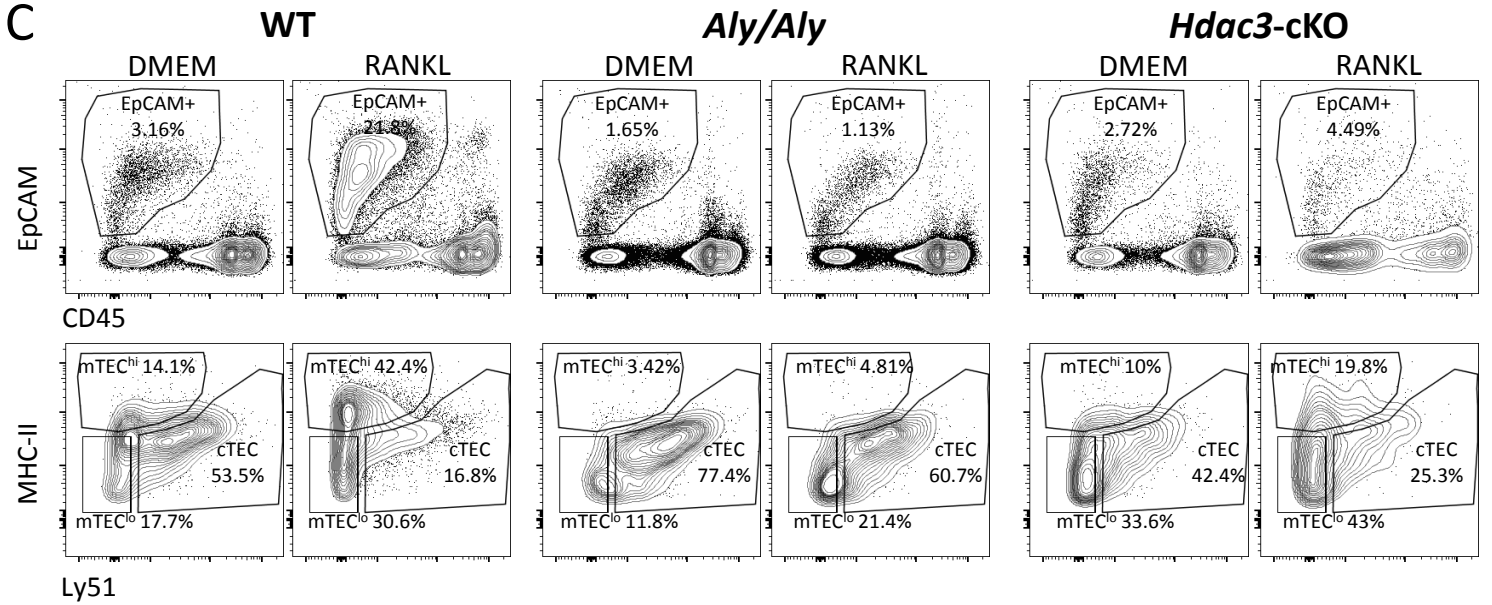
A



B



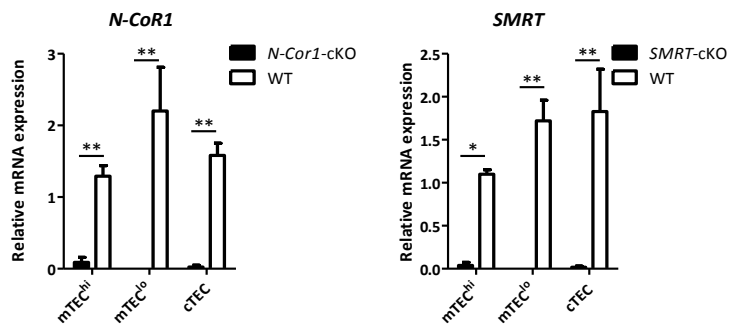
C



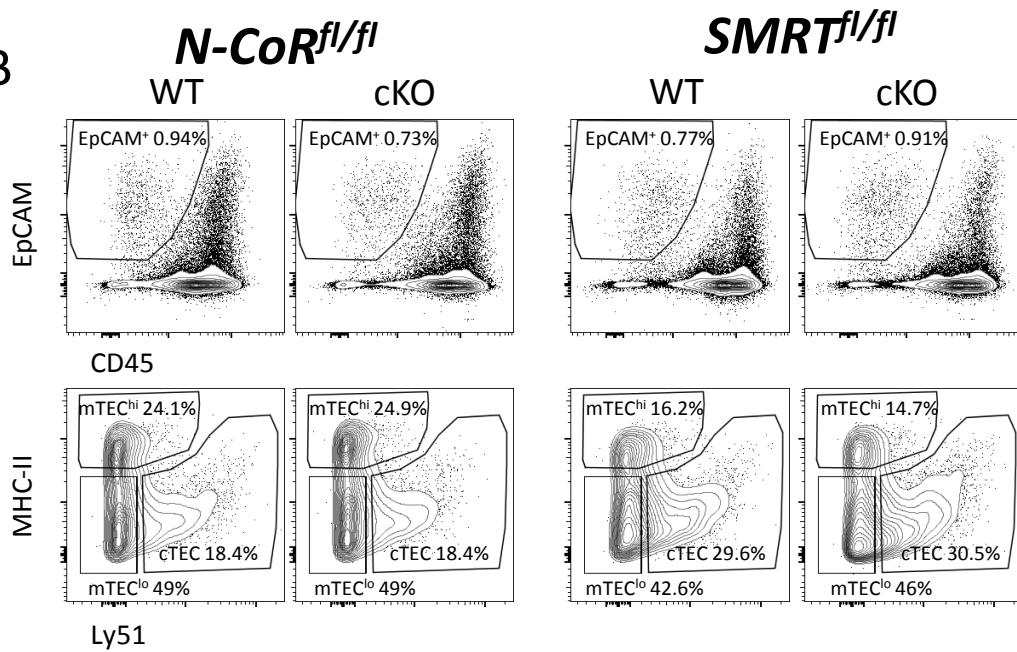
Suppl. Figure 3, related to Figure 3. (a) Representative flow cytometric profile showing frequencies of individual TEC populations from the mice indicated in Fig 3C. The displayed cells were first gated on CD45⁻EpCAM⁺ cells (Fig. 3C) and then analyzed according to CD80 and Ly51 expression to depict medullary (mTEC) and cortical (cTEC) populations. Individual gates indicate cortical (cTECs) and medullary (mTECs) epithelial cells either high (mTEC^{hi}) or dim (mTEC^{lo}) for CD80 (upper panel) and MHC-II (lower panel) molecule expression **(b)** Total cell numbers of the TEC and mTEC compartments of *Aly*^{+/-} and *Aly/Aly* mice. **(c)** Representative flow cytometric profiles of Fetal Thymic Organ Cultures (FTOCs) prepared from thymi isolated from E16.5-old WT, *Hdac3*-cKO and *Aly/Aly* embryos. The FTOCs were cultured for 7 days either in the absence (DMEM) or presence of soluble recombinant RANKL (1250ng/ml). Cells were first gated on CD45⁻EpCAM⁺ cells (upper panel) and were then gated according to Ly51 and MHC-II expression (lower panels). Individual gates indicate cortical (cTECs) and medullary (mTECs) epithelial cells either high (mTEC^{hi}) or dim (mTEC^{lo}) for MHC-II molecule expression.

Figure S4. Related to Figure 4

A

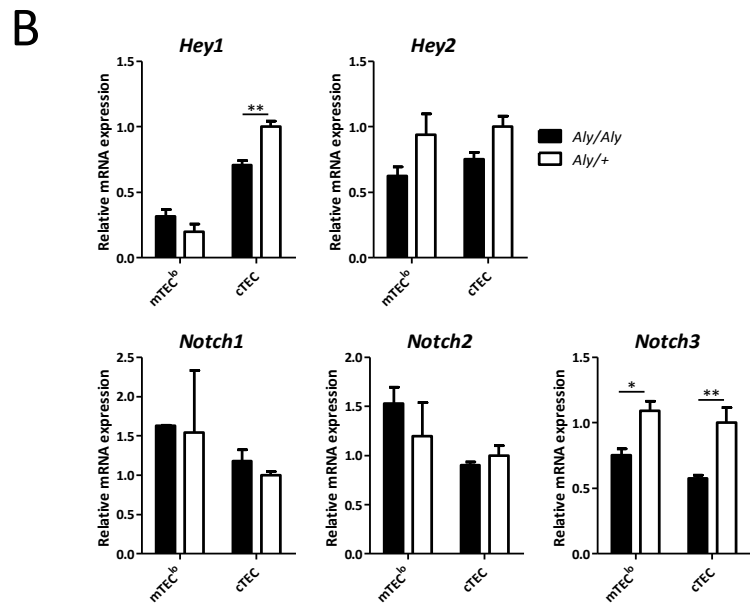
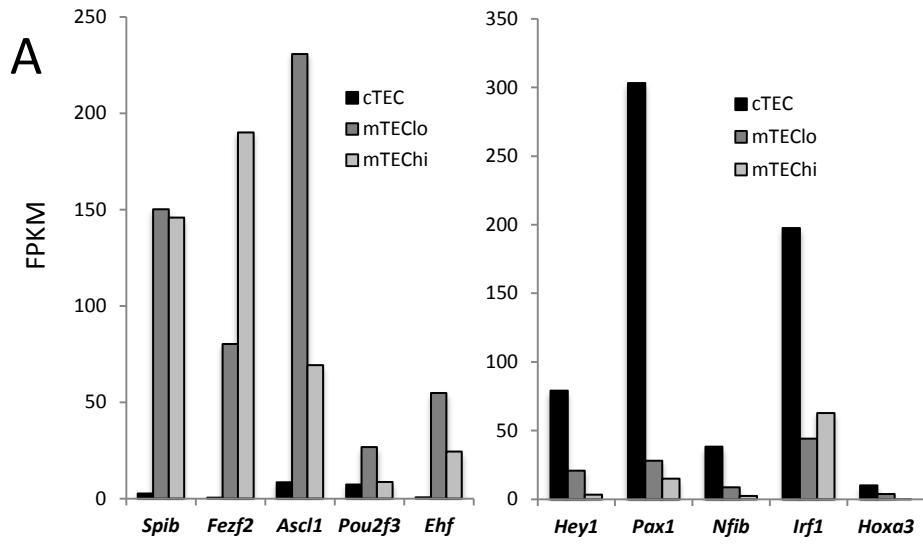


B



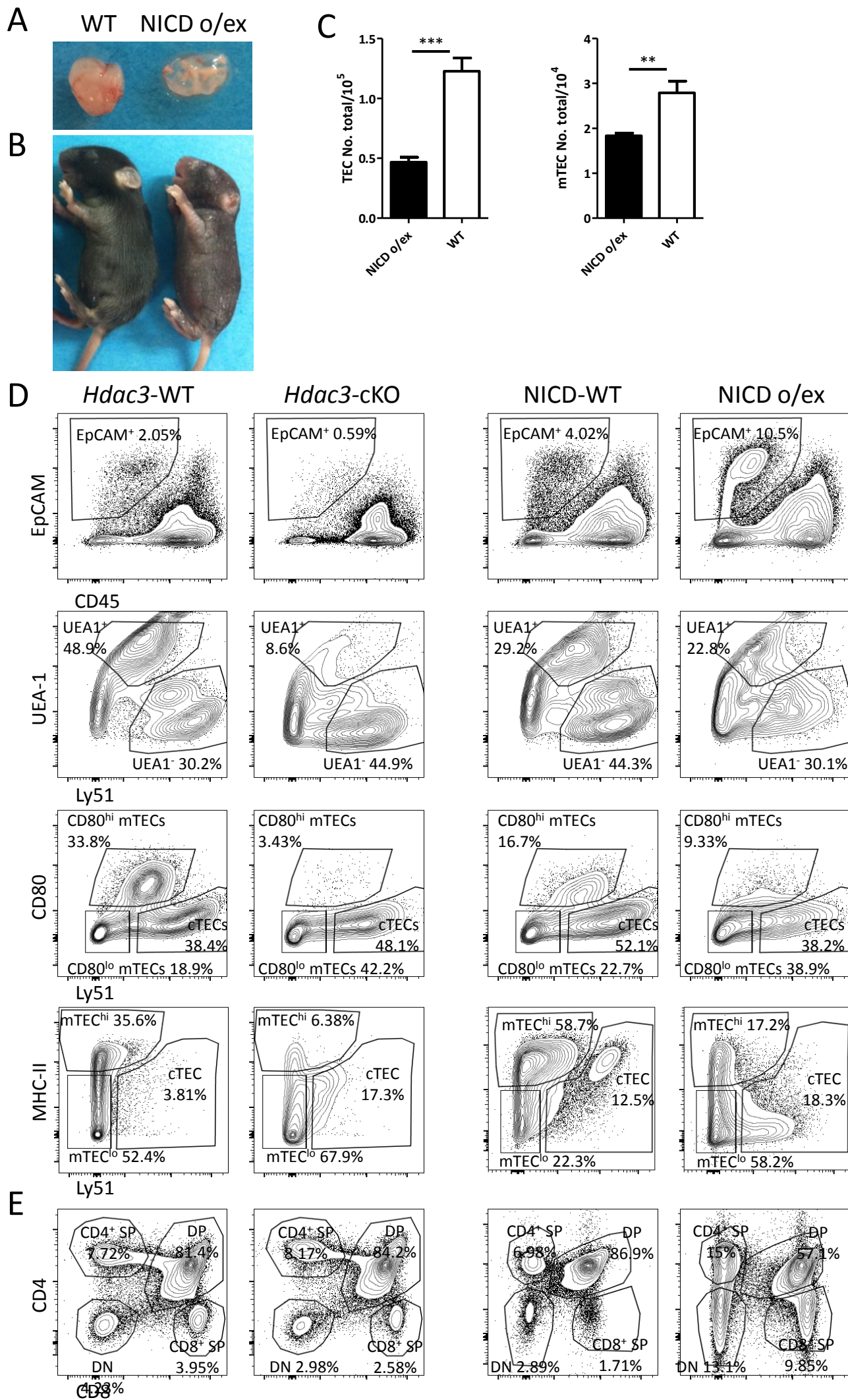
Suppl. Figure 4, related to Figure 4. (a) qPCR analysis of *Foxn1*.Cre-mediated recombination efficacy of *N-CoR1^{fl/fl}* and *SMRT^{fl/fl}* loci. Shown is relative mRNA expression + SEM of WT *N-CoR1* and *SMRT* in sorted mTEC^{hi}, mTEC^{lo} and cTEC populations isolated from either *Foxn1*.Cre-negative (WT; white) or *Foxn1*.Cre-positive (cKO, black) *N-CoR1^{fl/fl}* or *SMRT^{fl/fl}* mice. Data were normalized to *Hprt* mRNA levels. Asterisks indicate significant differences (*p < 0.05, **p < 0.001). (b) Representative flow cytometric profiles of WT and *N-CoR1* or *SMRT* individual cKO. Cells were first gated on CD45-EpCAM⁺ cells (upper panel) and were then gated according to Ly51 and MHC-II expression (lower panels). Individual gates indicate cortical (cTECs) and medullary (mTECs) epithelial cells either high (mTEC^{hi}) or dim (mTEC^{lo}) for MHC-II molecule expression.

Figure S5. Related to Figure 5



Suppl. Figure 5, related to Figure 5. (a) Expression of genes encoding mTEC specific (left panel) or cTEC specific (right panel) *Hdac3*-dependent TFs in mTEC^{hi}, mTEC^{lo} and cTECs, assessed by RNA sequencing and presented as fragments per kilobase of transcript per million mapped reads (FPKM). (b) Quantitative Real-Time PCR analysis assessing expression of a number of Notch pathway related genes in sorted mTEC^{lo} and cTEC cells isolated from *Aly*/⁺ (white) or *Aly*/*Aly* mice (black); data were normalized to *Hprt* mRNA levels and presented as percent of expression in WT cTEC; Asterisks indicate significant differences (*p < 0.05 and **p < 0.001).

Figure S6. Related to Figure 6



Suppl. Figure 6, related to Figure 6. (a) Thymi isolated from 10d old Rosa.flox-STOP-flox-NICD^{Foxn1.Cre-} (WT) and Rosa.flox-STOP-flox-NICD^{Foxn1.Cre+} (NICD o/ex) (b) Picture of 10d old Rosa.flox-STOP-flox-NICD^{Foxn1.Cre-} (WT) and Rosa.flox-STOP-flox-NICD^{Foxn1.Cre+} (NICD o/ex) mice showing skin phenotype caused by *Foxn1*-dependent Notch1 over-activation in keratinocytes and hair follicles. (c) Total cell numbers of the TEC and mTEC compartments of WT and NICD o/ex mice. (d) Representative flow cytometric profiles of dispersed thymic epithelial cell populations from 6-week-old *Hdac3*-WT, *Hdac3*-cKO, NICD-WT and NICD o/ex mice. Cells were first gated on CD45⁺EpCAM⁺ cells (upper panels) and were then either gated according to Ly51 and UEA-1 expression (middle panels), or according to CD80 or MHC-II and Ly51 expression (lower panels). Individual gates indicate cortical (cTECs, Ly51⁺UEA-1⁻) and medullary (mTECs, Ly51^{neg/lo}UEA-1⁺) epithelial cells either high (mTEC^{hi}) or dim (mTEC^{lo}) for CD80 and MHC-II molecule expression. (e) Representative flow cytometric profiles of CD4/CD8 thymocyte populations from 6-week-old *Hdac3*-WT, *Hdac3*-cKO, NICD-WT and NICD o/ex mice.

Suppl. Table 1

Top50 transcription factors induced by HDAC3 in mTECs						
Probe Set ID	Gene Symbol	mRNA Accession	WT	HDAC3cKO	WT/KO ratio	
10592705	Pou2f3	NM_011139	4162.5	332.2	12.5	
10371578	Ascl1	NM_008553	7783.4	639.7	12.2	
10543362	<i>Fezf1</i>	NM_028462	1084.6	101.3	10.7	
10417620	Fezf2	NM_080433	2938.3	358.8	8.2	
10485445	Ehf	NM_007914	2305.3	303.3	7.6	
10462575	<i>Lipm</i>	NM_023903	705.5	93.8	7.5	
10344679	<i>St18</i>	NM_173868	805.4	114.0	7.1	
10346168	<i>Stat4</i>	NM_011487	1119.2	174.2	6.4	
10354777	<i>Satb2</i>	NM_139146	975.5	155.4	6.3	
10540401	<i>Lrrn1</i>	NM_008516	929.5	151.3	6.1	
10416251	<i>Egr3</i>	NM_018781	3066.0	523.0	5.9	
10558580	<i>Utf1</i>	NM_009482	867.2	153.8	5.6	
10400504	<i>Foxa1</i>	NM_008259	931.6	207.3	4.5	
10494672	<i>Tbx15</i>	NM_009323	220.7	49.4	4.5	
10432032	<i>Vdr</i>	NM_009504	1706.1	407.1	4.2	
10356593	<i>Hes6</i>	NM_019479	2549.2	612.4	4.2	
10349993	<i>Myog</i>	NM_031189	427.3	105.4	4.1	
10361023	<i>Prox1</i>	NM_008937	473.4	118.0	4.0	
10571601	<i>Pdlim3</i>	NM_016798	3352.7	961.4	3.5	
10549276	<i>Bhlhe41</i>	NM_024469	1069.6	310.2	3.4	
10490755	<i>Hnf4g</i>	NM_013920	240.9	72.3	3.3	
10358027	<i>Elf3</i>	NM_001163131	3618.6	1093.1	3.3	
10350594	<i>Ivns1abp</i>	NM_054102	7126.5	2200.4	3.2	
10575763	<i>Gan</i>	NM_001081151	1027.6	323.1	3.2	
10603116	<i>Asb11</i>	NM_026853	264.2	84.2	3.1	
10510422	<i>Casz1</i>	NM_001159344	720.8	234.5	3.1	
10562812	Spib	NM_019866	4599.3	1586.1	2.9	
10515590	<i>Kdm4a</i>	NM_001161823	3296.2	1158.7	2.8	
10352576	<i>Esrrg</i>	NM_011935	377.7	133.2	2.8	
10404389	<i>Irf4</i>	NM_013674	472.4	167.2	2.8	
10489961	<i>Nfatc2</i>	NM_010899	736.5	263.5	2.8	
10569385	<i>Ascl2</i>	NM_008554	181.5	66.0	2.8	
10419966	<i>Zfhx2</i>	NM_001039198	642.2	241.8	2.7	
10473809	<i>Sfpi1</i>	NM_011355	1018.2	392.6	2.6	
10569102	<i>Irf7</i>	NM_016850	3286.9	1270.4	2.6	
10381172	<i>Stat5a</i>	NM_011488	1428.8	552.7	2.6	
10514347	<i>Cdkn2b</i>	NM_007670	803.8	325.4	2.5	
10451763	<i>Satb1</i>	NM_009122	1555.0	643.7	2.4	
10422013	<i>Klf12</i>	NM_010636	512.9	214.1	2.4	
10416800	<i>Lmo7</i>	NM_201529	734.4	307.4	2.4	
10481304	<i>Gfi1b</i>	NM_008114	593.1	250.9	2.4	
10545921	<i>Mxd1</i>	NM_010751	2558.9	1098.0	2.3	
10349295	<i>Tcfcp2l1</i>	NM_023755	805.7	358.5	2.2	
10536483	<i>Tes</i>	NM_207176	1879.6	849.4	2.2	
10532907	<i>Hnf1a</i>	NM_009327	360.7	163.0	2.2	
10363735	<i>Egr2</i>	NM_010118	3495.3	1602.5	2.2	
10565292	<i>Arnt2</i>	NM_007488	599.0	285.8	2.1	
10361828	<i>Cited2</i>	NM_010828	5755.6	2765.0	2.1	
10393266	<i>Foxj1</i>	NM_008240	234.2	114.5	2.0	
10404402	<i>Foxq1</i>	NM_008239	677.0	342.6	2.0	
10345016	<i>Tcfap2b</i>	NM_009334	105.6	55.3	1.9	

Suppl. Table 1

Top50 transcription factors repressed by HDAC3 in mTECs						
Probe Set ID	Gene Symbol	mRNA Accession	WT	HDAC3cKO	WT/KO	ratio
10505911	<i>Dmrta1</i>	NM_175647	342.0	3388.1		0.10
10423971	<i>Pkhd11</i>	NM_138674	100.1	925.0		0.11
10608107	<i>Uty</i>	NM_009484	93.2	614.3		0.15
10394534	<i>Osr1</i>	NM_011859	220.5	1413.8		0.16
10607972	<i>Kdm5d</i>	NM_011419	95.6	477.6		0.20
10474295	<i>Wt1</i>	NM_144783	145.4	718.5		0.20
10514049	<i>Nfib</i>	NM_001113209	227.4	989.3		0.23
10497203	Hey1	NM_010423	1161.3	5043.3		0.23
10368556	Hey2	NM_013904	403.9	1713.6		0.24
10421950	<i>Dach1</i>	NM_007826	179.4	700.8		0.26
10453857	<i>Gata6</i>	NM_010258	299.5	1091.1		0.27
10538811	<i>Prdm5</i>	NM_027547	220.3	791.9		0.28
10544751	<i>Hoxa2</i>	NM_010451	240.7	864.2		0.28
10601519	<i>Klhl4</i>	NM_172781	64.8	213.7		0.30
10380660	<i>Hoxb2</i>	NM_134032	162.3	513.7		0.32
10481056	Notch1	NM_008714	2659.7	8390.4		0.32
10363901	<i>Etv5</i>	NM_023794	188.3	577.8		0.33
10381006	<i>Thra</i>	NM_178060	677.3	2050.6		0.33
10376060	<i>Irf1</i>	NM_008390	2390.3	7034.3		0.34
10509218	<i>Zfp46</i>	NM_009557	288.3	834.9		0.35
10438626	<i>Etv5</i>	NM_023794	102.7	292.4		0.35
10476939	<i>Gm4979</i>	NM_001142411	532.8	1493.1		0.36
10600093	<i>Zfp185</i>	NM_009549	146.2	408.6		0.36
10544756	<i>Hoxa3</i>	NM_010452	91.8	255.2		0.36
10481857	<i>Pbx3</i>	NM_016768	709.1	1959.4		0.36
10374727	<i>Bcl11a</i>	NM_016707	834.6	2223.0		0.38
10390328	<i>Tbx21</i>	NM_019507	278.8	728.5		0.38
10488459	<i>Zfp442</i>	NM_001177550	70.5	182.7		0.39
10511835	<i>Fhl5</i>	NM_021318	56.6	146.4		0.39
10401238	<i>Zfp36l1</i>	NM_007564	2137.8	5505.4		0.39
10497646	<i>Phc3</i>	NM_001165954	384.8	987.2		0.39
10509163	<i>Id3</i>	NM_008321	1055.4	2699.6		0.39
10369252	<i>Sep10</i>	NM_001024911	381.1	953.0		0.40
10366293	<i>Csrp2</i>	NM_007792	1103.1	2721.4		0.41
10375864	<i>Agxt2l2</i>	NM_028398	406.5	992.9		0.41
10476874	<i>Pax1</i>	NM_008780	1550.8	3755.1		0.41
10386394	<i>Zfp867</i>	NM_178417	86.1	207.9		0.41
10459905	<i>Setbp1</i>	NM_053099	716.4	1726.3		0.42
10536505	<i>Met</i>	NM_008591	266.5	641.5		0.42
10395409	<i>Meox2</i>	NM_008584	544.6	1310.2		0.42
10529875	<i>Ldb2</i>	NM_001077398	584.1	1384.3		0.42
10557211	<i>Rbbp6</i>	NM_011247	150.0	355.2		0.42
10540523	<i>Lmcd1</i>	NM_144799	318.3	751.3		0.42
10565204	<i>Bnc1</i>	NM_007562	227.4	535.6		0.42
10506050	<i>Nfia</i>	NM_001122952	761.4	1787.7		0.43
10441270	<i>Ripk4</i>	NM_023663	410.2	938.6		0.44
10386219	<i>Zfp39</i>	NM_011758	236.8	541.8		0.44
10445071	<i>Zfp57</i>	NM_001013745	250.5	569.5		0.44
10434806	<i>Lpp</i>	NM_178665	2612.7	5811.1		0.45
10462195	<i>Kank1</i>	NM_181404	302.3	671.0		0.45

Supplemental Experimental Information

Extended Materials and Methods:

Antibodies and reagents:

Antibodies were purchased from the indicated manufacturers/providers:

eBioscience:

Fixable Viability Dye eFluor® 506

Vector laboratories:

Biotinylated UEA1

Biolegend:

APC, APC-Cy7 anti-mouse EpCAM (CD326)

FITC, PerCP-Cy5.5 anti-mouse CD45

Streptavidin conjugated PE-Cy7

PE, Biotinylated anti-mouse Ly51

Pacific-Blue, APC anti-mouse I-A/I-E

Pacific-Blue anti-mouse CD80

APC anti-mouse CD8 α

Pacific-Blue anti-mouse CD4

PE anti-mouse CD25

Alexa-Fluor 488 anti-mouse Foxp3

PE anti-rat IgG2c

Jackson:

Goat anti-Rabbit AF488

Goat anti-Rat Cy3

Streptavidin conjugated Cy2

Covance:

Rabbit polyclonal antibody anti-Keratin 5 (PRB-160P)

MBL:

Rabbit anti-Mouse β 5t

Millipore:

Rat anti-Aire mAb, clone 5H12

Recombinant mouse RANKL was produced by the Structural Proteomics Unit at the Weizmann Institute.

Cell preparation, flow cytometry and sorting:

A) Isolation of thymic stromal cells: Thymi were surgically removed from mice of different ages (2 – 16 weeks) and placed into cold 1X PBS supplemented with 2% Fetal Bovine Serum (FBS, Invitrogen). Thymi were trimmed of fat and connective tissues and minced into small pieces. Thymi were then disintegrated by enzymatic digestion using 0.5mg/ml Collagenase D (Roche #1088858), 1mg/ml Collagenase-Dispase cocktail (Roche #269638), 2% FBS and DNase in RPMI until complete digestion.

The single cell suspension was then filtered through 52micron mesh filter and resolved on a Percoll gradient. To this end, single cell suspension was washed and re-suspended in 1.115 g/ml isotonic Percoll (Sigma), topped by one layer of isotonic 1.065 g/ml Percoll and one layer of 1X PBS. Percoll gradient was centrifuged at 2700rpm at 4°C with no break, for 30 minutes. Stromal cells, found between the 1X PBS layer and the 1.065 g/ml Percoll layer, were collected and washed with MACS buffer (2% FBS with 5mM EDTA pH 8.0 in 1X PBS) followed by centrifugation at 1300rpm for 4 minutes at 4°C. Cells were then stained with the specific antibodies.

B) Isolation of thymocytes: Thymi were mechanically digested by squashing through a 40micron cell strainer. Thymocytes were collected into MACS buffer, filtered again through 52micron mesh filter, washed with MACS buffer and subjected to staining with the appropriate antibodies.

C) Isolation of splenocytes: Spleens were surgically removed from 4- to 9-week-old mice and placed into cold 2% FBS in 1X PBS. Spleens were then trimmed of fat and connective tissues and then mechanically disintegrated through 40µm mesh filter. Cells were collected and washed with MACS buffer. In order to remove red blood cells, pellets were re-suspended in 1X ACK Lysing buffer (15mM Ammonium-Chloride, 1mM Potassium bicarbonate, 10µM EDTA in DDW, pH 7.3) and incubated for 4 minutes in room temperature. After incubation, cell suspension was washed with MACS buffer, filtered through 52 micron mesh filter, washed again and then stained with the specific antibodies.

Immunostaining of cell suspensions: All cells were stained in 100µl MACS buffer and incubated with the specific fluorophore-labeled antibodies for 20-60 minutes at 4°C. Antibodies and dilutions are indicated under antibodies section.

For intracellular staining of Aire or Foxp3, cells labeled for membrane antigens were washed

and then fixed in Fixation/Permeabilization solution (eBioScience/ Biolegend, respectively), followed by Aire/anti-rat IgG2c-PE staining or Foxp3-Alexa 488 antibody staining.

Flow cytometry analysis, sorting and data processing:

Following staining, cells were washed, re-suspended in MACS buffer, filtered and analyzed either on the BD FACS Canto II analyzer or sorted in BD FACS Aria III cell sorter. All compensations were performed on cells labeled with single colors. Data analysis was done using FlowJo software.

Real-Time PCR analysis:

RNA was extracted from sorted cells using Trizol reagent and used for cDNA synthesis (Life Technologies) according to manufacturer’s instructions and the entire amount of purified total RNA was then used for cDNA synthesis using the High-Capacity cDNA kit (Applied Biosystems) and random primers. The subsequent qPCR analysis was performed using the Fast SYBR Green Master Mix (Life technologies) or TaqMan Fast advanced master mix (Life technologies) for testing deletion efficacy. Differential expression was calculated according to the $\Delta\Delta CT$ method and the obtained data were then statistically evaluated (ANOVA test, P-value < 0.05) using StatView software (SAS Institute Inc.).

List of specific TaqMan assays for deletion efficacy:

All assays were purchased from ThermoScientific

Mouse strain	Assay ID
<i>Hdac1</i> -flox	Mm01610894_g1
<i>Hdac2</i> -flox	Mm01193629_m1
<i>Hdac3</i> -flox	Mm01258398_g1
<i>N-CoR1</i> -flox	Mm01333098_m1
<i>SMRT</i> -flox	Mm01198135_m1

List of specific primers for qPCR analysis:

Gene	Forward	Reverse
Rpl32	TTAAGCGAAACTGGCGGAAAC	TTGTTGCTCCCATAACCGATG
HPRT	TGAAGAGCTACTGTAATGATCAGTCAA	AGCAAGCTTGCAACCTTAACCA
Aire	GTACAGCCGCCTGCATAGC	CCCTTTCCGGGACTGGTT
Ins2	GACCCACAAGTGGCACAA	ATCTACAATGCCACGCTTCTG
Pcp4	TCTGAGCTGTTCTGTGGGACC	TCCGGCACTTTGTCTCTCACT

Mup4	CTGACCCTAGTCTGTATTCATGCA	CCATTCCCCATTAATCTTTTCTACATT
Dio1	TGCTACAAGGGTAAAGCTGGCCC	AGGCACGTGTCTAGGTGGAGTG
Zp2	GGGCTCTCCAGCCTGATCTACTTC	ATGCAGGGCAAGTCACAGAGC
Pld1	AGTGCAGTTGCTCCGATCTGC	TGGATGTAGGCAGCGTGGATGG
RANK	AGAGGCATTATGAGCATCTCG	GGAGTGCACCTTAGAGGACAGGT
IkBα	ACGAGCAAATGGTGAAGGAG	ATGATTGCCAAGTGCAGGA
RelB	CCGGCACAGCTTTAACAACC	TCTTCAGGGAGCCAGCATTG
Fezf2	ACTCGGCCTGACAGCTGAACG	TGAGCATTGAACACCTTGCCGCAC
Ascl1	TGGACTTTGGAAGCAGGATGG	GAAGGTGCCCCTGTAGGTTG
Pou2f3	CCATGCCTGGAACAGTAACG	CCTGAACCAGGAGACGAAGG
Hey1	TGAGAAGCAGGGATCTGCTAAG	GCATTCCCGAAACCCCAAAC
Hey2	ACAGGGGGTAAAGGCTACTTTG	AGATGAGAGACAAGGCGCAC
Notch1	ACAGTGCAACCCCCTGTATG	AGTTGTTCCGTAGCTGGTCG
Notch2	GCCACTGCATGTTGCCTTAC	CATCGTTTACCTTGCCAGCC
Notch3	TTCCCCGTGTCGTAATGGTG	TCGAAGCCAGGAAGGCAAG
Pax1	CGGACGTTTATGGAGCAAAC	TCCATCTTGGGGGAGTAGG
Prss16	TGGGACGTCAGAAAATCTCCC	TGATGGGACTGTCAAAGGGC
Sp1B	ATCTCAGGCAGGTGCACGCAAG	GCGAGCCAACAACCTCCTTGTGC
CD40	GAGTCAGACTAATGTCATCTGTGGTT	GGTTTCTTGACCACCTTTTTGA

Pathological evaluation and mice irradiation:

Histopathology, including analysis and scoring of immune infiltrates in various peripheral tissues, was performed under supervision of a certified animal pathologist. Briefly, scoring was assessed according to size and frequency of immune infiltrates, with scanning of 3 slices from each animal. Score 0 marked animals in which no infiltrates were found, while score 2.5 marked animals in which many large infiltrates were found (Suppl. Fig. 2B). Final score was calculated as the average of scoring performed by two independent people.

Hdac3-cKO and WT mice (5 to 6-week-old) were sub-lethally irradiated (~300 rad) in order to cause transient lymphopenia, as a means to aggravate autoimmunity. Mice were analyzed three months later for the presence of immune infiltrates in peripheral tissues, as described above.

Statistical analysis:

Two- or three-way analysis of variance (ANOVA) with a pre-determined significance level of 0.05 was conducted. Provided significant group differences, Fisher's protected least significant differences (Fisher's PLSD) contrasts were performed to compare specific pairs of

groups. Student's t-test was used for the comparison of only two groups to determine statistically significant differences with a pre-determined significance level of 0.05. The Mann-Whitney U-test for unpaired samples was used to determine the statistical significance of autoimmune infiltrates with a pre-determined significance level of 0.05. All statistical analyses were conducted using StatView software (SAS Institute, San Francisco, CA).